Journal of Applied Physics

RESEARCH ARTICLE | MARCH 15 2024

Undoing band anticrossing in highly mismatched alloys by atom arrangement

Special Collection: Native Defects, Impurities and the Electronic Structure of Compound Semiconductors: A Tribute to Dr. Wladyslaw Walukiewicz

Qian Meng ; Seth R. Bank ; Mark A. Wistey

J. Appl. Phys. 135, 113101 (2024)
https://doi.org/10.1063/5.0179255

25 March 2024 19:09:40

Boost Your Optics and Photonics Measurements
Lock-in Amplifier
Zurich Instruments
Find out more
Boxcar Averager

Journal of Applied Physics | ARTICLE | pubs.aip.org/aip/jap

Undoing band anticrossing in highly mismatched alloys by atom arrangement

Cite as: J. Appl. Phys. **135**, 113101 (2024); doi: 10.1063/5.0179255
Submitted: 30 September 2023 · Accepted: 27 February 2024 ·
Published Online: 15 March 2024

Qian Meng,[1] Seth R. Bank,[1] and Mark A. Wistey[2,3,a)]

AFFILIATIONS

[1]Microelectronics Research Center and Department of ECE, The University of Texas at Austin, Austin, Texas 78758, USA
[2]Materials Science, Engineering, and Commercialization Program, Texas State University, San Marcos, Texas 78666, USA
[3]Department of Physics, Texas State University, San Marcos, Texas 78666, USA

Note: This paper is part of the Special Topic on Native Defects, Impurities and the Electronic Structure of Compound Semiconductors: A Tribute to Dr. Wladyslaw Walukiewicz.
[a)]**Author to whom correspondence should be addressed:** mwistey@txstate.edu

ABSTRACT

The electronic structures of three highly mismatched alloys (HMAs)—GeC(Sn), Ga(In)NAs, and BGa(In)As—were studied using density functional theory with HSE06 hybrid functionals, with an emphasis on the local environment near the mismatched, highly electronegative atom (B, C, and N). These alloys are known for their counterintuitive reduction in the bandgap when adding the smaller atom, due to a band anticrossing (BAC) or splitting of the conduction band. Surprisingly, the existence of band splitting was found to be completely unrelated to the local displacement of the lattice ions near the mismatched atom. Furthermore, in BGaAs, the reduction in the bandgap due to BAC was weaker than the increase due to the lattice constant, which has not been observed among other HMAs but may explain differences among experimental reports. While local distortion in GeC and GaNAs was not the cause for BAC, it was found to enhance the bandgap reduction due to BAC. This work also found that mere contrast in electronegativity between neighboring atoms does not induce BAC. In fact, surrounding the electronegative atom with elements of even smaller electronegativity than the host (e.g., Sn or In) consistently decreased or even eliminated BAC. For a fixed composition, moving Sn toward C and In toward either N or B was always energetically favorable and increased the bandgap, consistent with experimental annealing results. Such rearrangement also delocalized the conduction band wavefunctions near the mismatched atom to resemble the original host states in unperturbed Ge or GaAs, causing the BAC to progressively weaken. These collective results were consistent whether the mismatched atom was a cation (N), anion (B), or fully covalent (C), varying only with the magnitude of its electronegativity, with B having the least effect. The effects can be explained by charge screening of the mismatched atom's deep electrostatic potential. Together, these results help explain differences in the bandgap and other properties reported for HMAs from different groups and provide insight into the creation of materials with designer properties.

© 2024 Author(s). All article content, except where otherwise noted, is licensed under a Creative Commons Attribution (CC BY) license (http://creativecommons.org/licenses/by/4.0/). https://doi.org/10.1063/5.0179255

25 March 2024 19:09:40

I. INTRODUCTION

The incorporation of isoelectronic impurities that are highly mismatched with host structure, i.e., size and electronegativity, has gained wide interest after the pioneering work of Shan *et. al* and Wu *et al.*,[1,2] because of the design freedom spanning a large range of bandgap and lattice constants.[3–12] These provide new opportunities for optoelectronics spanning a large wavelength range and lattice match to Si/GaAs simultaneously. In contrast to traditional alloys like GaAs, the properties of highly mismatched alloys (HMAs) cannot be predicted using the virtual crystal approximation (VCA), in which the properties are determined by the weighted average of the alloy endpoints.[13] For example, adding N to GaAs decreases the lattice constant, as expected, but it also sharply *decreases* the bandgap,[14,15] while the VCA would predict the bandgap increasing toward that of GaN.

Many phenomenological models have been developed to explain the counterintuitive change in the bandgap, including band anticrossing (BAC),[1,2] the hybridization of L-related states,[16,17] the interaction between localized clusters and host,[18,19] or a

combination of the N cluster and BAC model.[20,21] Among these, the rather simple BAC model successfully explained the significant reductions in the bandgap and electron mobilities, and increased effective mass in dilute nitrides.[2,14,22,23] In the BAC model, with a strongly electronegative impurity, as studied here, the mismatched atoms strongly attract and at least partly localize the electron wavefunction near themselves, resulting in a new state, localized in real space and extending across in reciprocal space. The interaction of this new state with the host's original Bloch-like conduction band results in mutual repelling of the two, which can significantly affect the bandgap of the alloy.[1,2,24,25] Electropositive impurities such as Bi in GaP similarly affect the valence band.[26,27] Nevertheless, the original BAC model, with a constant defect energy level across the Brillouin zone (BZ), is incomplete: adequate band structures near the zone center but failing to predict band structures away from $k = 0$.[28] Notably, BAC and hybridization interpretations are not mutually exclusive. While the BAC model does have limits, as mentioned above, the present work shows that it applies at least as well in dilute HMAs discussed in this paper, particularly for properties near the zone center, which is our focus in this paper. As we show below, the strength of the energy splitting associated with BAC depends on the degree of localization near the "defect" atom, which is tunable by alloy composition and atom arrangement, among other things.

A simultaneous decrease in both the bandgap and the lattice constant in Group IV HMAs (GeC) was also verified by the theory and experiment,[10,28–30] similar to III–V HMAs with group V atom mismatched (GaInNAs). We have recently further explored HMAs in which the group III atom is mismatched, i.e., BGaAs. These were found to have a perturbation in the conduction band minimum (CBM) as well, although the BAC is much weaker, as previously predicted.[31–34]

However, *a priori* predictions of the effects of BAC, such as bandgap, are still inconsistent. For example, both increased and decreased bandgaps have been predicted for BGaAs,[16,34–40] while BAC definitively predicts a decrease in the CBM. The contradictory observations and their underlying origins have lacked a systematic study with a unifying explanation. This work sought to elucidate the origins of the discrepancy originating from the unique size mismatch effect of B, distinguishing it from other HMAs.

In addition, HMAs that include an additional, larger element with weaker electronegativity, such as in BGaInAs, GaInNAs, or GeCSn, frequently show a different bandgap from HMAs without the larger species, and the variation changes with anneal, presumably due to different atom distributions.[41,42] A few studies have offered possible explanations, ranging this, from energy level changes in different host structures,[43] changes in the coupling factor in different configurations,[42] to wavefunction mixing in the conduction band.[41] However, none of these made a direct connection from changed parameters, i.e., wavefunctions, to quantified results in relation to BAC, and most were difficult to generalize to other alloys. Moreover, the systematic exploration of blueshift mechanisms observed in BGaInAs during annealing has been largely absent in previous studies. Given the analogous blueshift observed in III–V HMAs, extending this analysis to group IV material systems like GeCSn could yield valuable insights for growth processes and experimental investigations. This work addresses the mechanisms behind the blueshift.

The goals of this study were to (1) understand and distinguish the origins of BAC in HMAs, separating electronegativity from atom size, strain, and lattice distortions; (2) study the limits of BAC in the limits of weak mismatch (B in GaAs) and compensating atoms (In, Sn); and (3) generalize these results to HMAs as a class.

In this study, the electronic structures of GeC(Sn), Ga(In)NAs, and BGa(In)As in different arrangements were studied using density functional theory (DFT) with hybrid functionals. We incorporated results from Ga(In)NAs due to its well-established theory and multiple experimental measurements in the literature. This choice serves as a valuable benchmark for comparison, aiding a deeper understanding of the other HMAs, particularly BGa(In)As and GeC(Sn). The ternaries GaNAs and BGaAs and binary GeC, each incorporating one single isolated mismatched atom, were first studied to investigate the strength of BAC in each material. We found that the bandgap decreases for GeC and GaNAs but increases in BGaAs where the main differences come from the strength of BAC and effects of structure distortion. Adding a less-electronegative atom, such as in GeCSn, BGaInAs, or GaInNAs, allowed tuning of both band splitting and bandgap depending on the atom arrangement.

In the following discussion, "distortion" refers to the local displacement of atoms from the perfect diamond or zincblende (ZB) lattice, particularly the change in local bond lengths near the mismatched atom. In addition, to avoid confusion with signs, "stronger" electronegativity here means larger in magnitude.

25 March 2024 19:09:40

II. METHODS

DFT calculations of GeC(Sn), Ga(In)NAs, and BGa(In)As in different arrangements were performed using the projector-augmented wave (PAW) method under the Vienna *Ab initio* Simulation Package (VASP).[44,45] The exchange and correlation were enabled by hybrid functional HSE06 to provide an accurate electronic structure and bandgaps with reasonable computational efficiency.[46–48] The lattice structures of the alloys were constructed using 128-atom supercells with zincblende structures. Plane waves with energies up to 1.5 times the largest cutoff energy were included. For GeC(Sn), Ga(In)NAs, and BGa(In)As, these values were set to be 600, 600, and 478 eV, respectively. The electronic convergence criterion was 10^{-8} eV for all supercells.[32,49] A Γ-centered, $2 \times 2 \times 2$ Monkhorst–Pack grid was used for 128-atom supercells to sample the Brillouin zone. Atom positions were relaxed over a range of supercell sizes (lattice constants), and the ground state system was obtained by fitting with the Birch–Murnaghan equation[50,51] followed by the re-relaxation of the structure under the lattice constant with the minimum system energy, unless otherwise noted. Electronic properties were extracted based on these optimized structures. When using supercells in DFT, the bands outside the first Brillouin zone (BZ) get folded into the first BZ, hindering a direct comparison of the band structure between different arrangements. BandUP[52–55] and PyVaspwfc[56] were used to unfold or project the band structure into the first Brillouin zone. Representative tests including spin–orbital coupling (SOC) found virtually no effect on the conduction band states where BAC

© Author(s) 2024

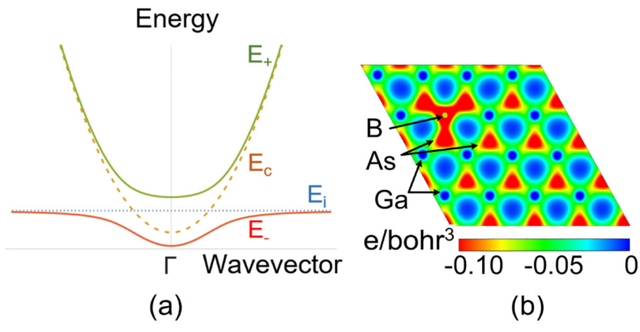

FIG. 1. (a) A sketch showing the anticrossing and hybridization of highly mismatched "impurity" state E_i with original conduction band E_C, forming E_- and E_+ bands. (b) Charge density map in the (110) plane shows localized charge near B in BGaAs.

occurs.[1,28,32] Therefore, SOC was not included here. In addition, unless otherwise noted, all strains reported herein are hydrostatic; the effects of biaxial strain, such as splitting the degeneracy of light and heavy holes, are the same as in traditional alloys, which are well understood.

III. RESULTS AND DISCUSSION

A. BAC and local distortion

Based on Hjalmarson's theory, the energy of isoelectronic impurities in the band structure is related to the atomic orbital energy.[57] The N in GaAs, B in GaAs, and C in Ge are predicted to each create a new state, shown as E_i in Fig. 1(a), that is located near the host's CB minimum. Since these states share the same s-like symmetry on each atom, they cannot share the same energy but instead show a band anti-crossing (BAC) or avoided crossing. The original CBM, perturbed by the localized state, hybridizes into E_+ and E_- states as shown in Fig. 1(a). Using BGaAs as an example, the charge distribution showed a strong charge peak around mismatched atoms in Fig. 1(b), indicating the localization of mismatched atoms. The strong charge peak around the C atom was also observed in dilute GeC.[28]

While BAC in GeC has recently been disputed,[29,30] it may be worth noting that BAC in the GeC CB may be strong at Γ without significantly affecting L or X.[28] Early BAC papers assumed that the energy of the isoelectronic impurity state and the interaction strength V between the bands are both constant across the entire Brillouin zone, rather than a function of k. However, if V is a function of k, strong near $k = 0$ and weaker with increasing $|k|$, then BAC would move the CB edge at Γ without necessarily affecting L or X. Indeed, we found a weak splitting toward L and none toward X, but a strong splitting in Γ in the $Ge_{127}C_1$ band structure, as shown in Fig. 2, indicating different interaction strengths. This leads to a direct bandgap with an optical transition strength in the same order as GaAs.[28] Strong optical transitions, significant Γ character, increased effective mass, and strain dependence of band energies that track the Γ CB valley but not the L valley, together strongly suggest that BAC applies to GeC as well as it does to GaAsN and BGaAs.[28] It is important to note that the aforementioned conclusion is from the analysis of a single, isolated C atom in an artificially ordered supercell. The properties of GeC may exhibit variations when considering larger carbon concentrations with alloy disorder.

Two types of perturbation are induced by mismatched atoms: size and electronegativity. The small-sized atom pulls neighboring atoms inward, inducing local bond distortion that deviates from the original host lattice positions. At the same time, the strong electronegativity of the mismatched species changes the wavefunction or charge distribution due to the differences in the combined potentials from the atom core and electron cloud.

The influences of the two types of perturbations were studied both separately and together using 128-atom supercells with a single mismatched atom (B, C, or N), as shown in Fig. 3(a). For (110) lattice structure sketches, Z atom represents B, C, or N. In

25 March 2024 19:09:40

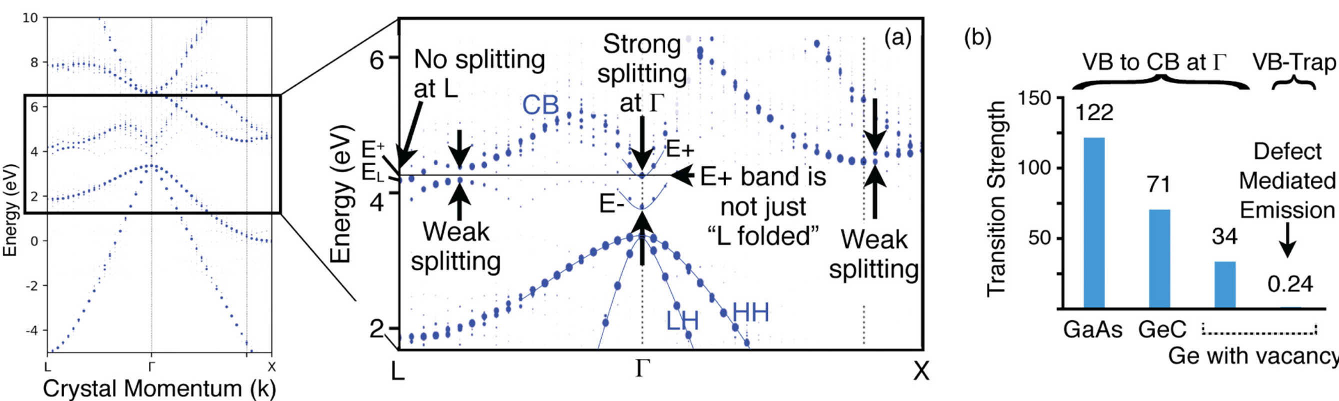

FIG. 2. (a) Unfolded band structure of $Ge_{127}C_1$. Strong CB splitting near Γ ($k = 0$), becoming weaker near edges of the first Brillouin zone. Size of dots represents similarity with states from ideal Ge. Solid lines are guides to the eye. Reprinted with permission from I. A. Gulyas *et al.*, J. Appl. Phys. **129**(5), 055701 (2021).[28] (b) Calculated optical transition strength from the VB to trap or CB states at Γ for 128-atom GaAs, Ge, and Ge with single vacancy. GeC shows strong optical transitions consistent with BAC.

© Author(s) 2024

BGaAs and GaAsN, X is Ga and Y is As. In GeC, X and Z are both Ge. The dashed circle is the original site of atoms in a perfect zincblende structure. The second row shows the band structures that result when the positions of atoms in Ge or GaAs were forced to match the positions of the corresponding HMAs (BGaAs, GeC, GaAsN) as sketched in axis labels for the second and fourth rows, copying the structure distortion of the HMA to the host but excluding the mismatched species. The third row shows the converse, in which the perfect diamond or ZB lattice host structure was frozen in place and a single atom of the mismatched species was substituted for the corresponding host atom, without allowing the atoms to relax, thus excluding structure distortion, as shown in axis labels for the first and third rows. The bottom row shows band structures of the fully relaxed HMAs, including both the mismatched atom and structure distortion. All configurations were studied considering one isolated mismatched atom. The blue circles highlight that BAC occurred if and only if the mismatched species were present, regardless of distortion in the lattice. On the other hand, the structure distortion without mismatched atoms restored a clean zone center nearly the same as the unperturbed host band structure.

The bandgap changes in the above configurations were then quantitively analyzed. For all three alloys, substituting a mismatched atom but rigidly maintaining the same lattice positions as the host (i.e., no relaxation) led to a decreased bandgap, as expected from BAC, as shown in the column under pure chemical in Fig. 3(b). For traditional alloys with a zincblende structure, a smaller lattice should result in a larger bandgap. Indeed, as shown in Fig. 3(b) in the column under pure distortion, the structure of pure GaAs and Ge has increased bandgaps when distorted to match the same atom positions as their respective HMAs BGaAs/GaAsN and GeC. In this case, the decrease in the overall lattice constant induced by adding a small, mismatched atom increases the bandgap, just as it does in traditional III–V alloys.

The strengths of BAC in different HMAs discussed above were then evaluated. In the BAC model, the magnitude of conduction band reduction is decided by the energies of the host CBM and the impurity, and the coupling factor V. The coupling factors were calculated using[1]

$$E_{\pm} = \left(E_N + E_M \pm \left[(E_N - E_M)^2 + 4V_{MN}^2\right]^{1/2}\right)/2, \quad (1)$$

where E_- and E_+ represent the energy levels of split bands after BAC; E_N and E_M denote the energy levels of the isoelectronic impurity and host, respectively, before anticrossing; and V_{MN} is the coupling factor that measures the strength of coupling between the impurity state and the host state.

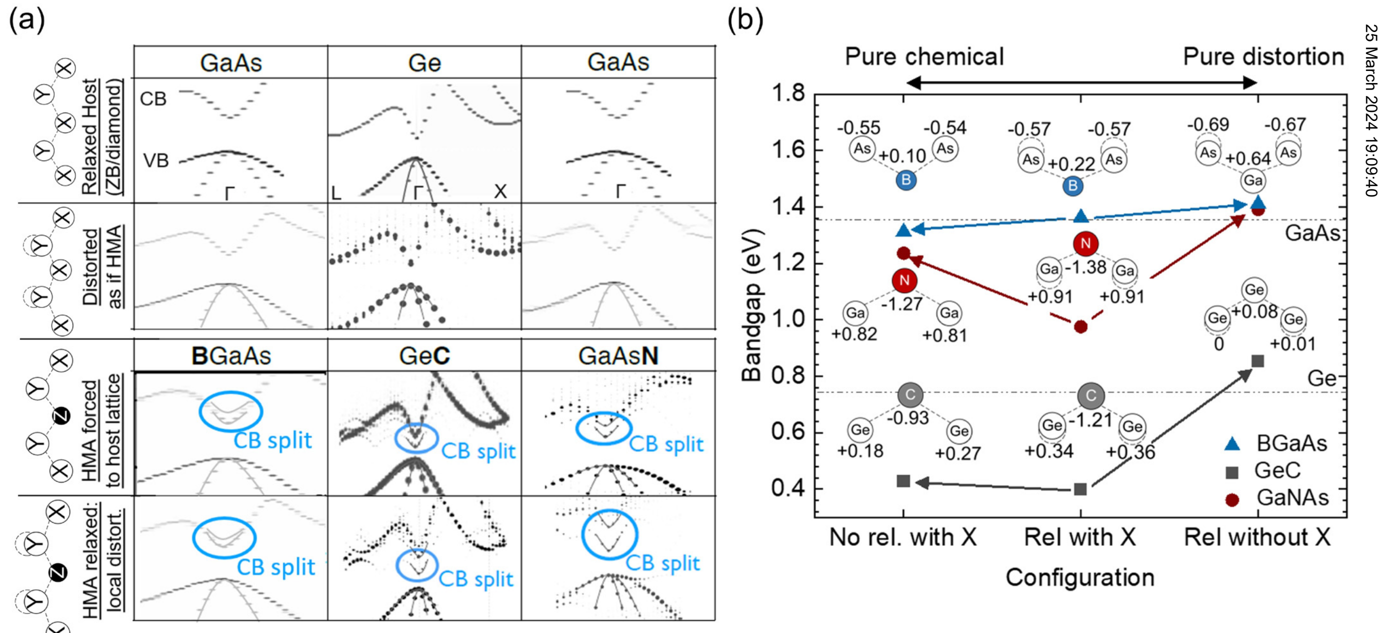

FIG. 3. (a) Band structures near the zone center for (B)GaAs, Ge(C), and GaAs(N), in a 128-atom supercell with single B, C, or N, treating mismatched atom electronegativity and structure distortion separately. Gray lines are parabolic guides to the eye near CB/VB band edges. X = Ga or Ge. Y = As or Ge. Z = B, C, or N. The dashed circle is the original site of atoms in a perfect zincblende (ZB) or diamond structure. The dashed circle is the original site of atoms in a perfect zincblende structure. (b) Bandgap corresponding to configurations in (a), where X is the mismatched atom (B, C, N) and rel. denotes relaxation. Numbers represent the Bader charge analysis with a unit of electron on the (110) plane, indicating the charge transfer in different configurations. Parts of (a) are reprinted with permission from Q. Meng *et al.* J. Appl. Phys. **132**(19), 193104 (2022) and I. A. Gulyas *et al.*, J. Appl. Phys. **129**(5), 055701 (2021).

25 March 2024 19:09:40

© Author(s) 2024

The energy levels of E_- and E_+ bands were obtained from the unfolded band structure calculations. The energy level of N impurity is used as 0.23 eV above the GaAs CBM as referenced by Wu *et al.*[2] The energies of B and C states were extracted by fitting the asymptotes of the E_+ and E_- bandgap with pressure. Specifically, the C state was positioned at 0.06 eV below the Γ valley of Ge,[28] while the B state was identified at 0.3 eV above the CBM of GaAs.[58] Finally, the coupling factor for each alloy was calculated.

The calculated coupling factor V was 0.13, 0.29, and 0.21 eV for unrelaxed BGaAs, GeC, and GaNAs [column pure chemical in Fig. 3(b)], respectively. In fully relaxed substitutional HMAs, where both the size mismatch and electronegativity mismatch exist, bond length distortion around mismatched atoms has a different effect in different HMAs. In strongly mismatched systems such as GeC and GaNAs, a distorted lattice with smaller local bonds and lattice constant can enhance the BAC, resulting in a further decreased bandgap than one without distortion, as seen comparing the column no rel. with X to column rel. with X in Fig. 3(b), similar to that shown in a previous GaNAs report.[59] As clearly seen in Fig. 3(a), the separation between the E_+ and E_- bands became more distinct with structural distortion. V largely increased at about two times to 0.49 eV in GaAsN when the local Ga bond length shrank by 15% from Ga–As to Ga–N. The increase in V was smaller in GeC, from 0.29 to 0.33 eV, with bond length decreasing by 14% from Ge–Ge to Ge–C. On the contrary, in BGaAs, which is the least mismatched of these alloys, even though the bond decreased similarly by ∼12% compared with GeC and GaNAs, the bandgap did not decrease. This appears to be due to the charge transfer between neighboring bonds involving mismatched atoms, i.e., from B to As, Ge to C, and Ga to N, which is easier if atoms are closer. As shown in Fig. 3(b), the Bader charge analysis indicated a stronger charge localization on C and N. In contrast, B does not pull as much charge from its neighbors. Only the nearest-neighbor atoms are shown since the perturbation on charge from the mismatched atom is essentially confined to their first-nearest-neighbor atoms.

For HMAs with weak BAC (for example, $V = 0.13$ eV for unrelaxed $B_{0.016}Ga_{0.984}As$), the reduction in the bandgap from BAC is less than the increase due to structure distortion. The change in the overall lattice constant due to the small size of boron increased the bandgap that was larger than the decreased bandgap due to weak BAC, resulting in an overall increased bandgap in relaxed BGaAs. The compensation of size mismatch (strain) and chemical mismatch (BAC) on the bandgap of BGaAs was first observed and unusual in this material system. The detailed discussion for BGaAs will be reported elsewhere.[58] The much weaker BAC in mixed-cation alloy BGaAs might be due to the structure symmetry difference between group III and group V sublattices[16] or much weaker electronegativity in group III elements compared with group V.[36] It could also be related to the charge variation in B, which is the smallest among three mismatched atoms. The atom with the strongest electronegativity will pull the electrons toward itself where the process is much easier for anion (N) or covalent bond (C) alloys. However, the B atom in BGaAs is expected to be a cation and give electrons to the As atom, mitigating the ability for it to pull more electrons from As. The effects of size and electronegativity in the band structure for C, N, and B suggested two ways to manipulate the localization stemming from the mismatched atom and consequently tuning the behavior of BAC: (1) varying the local bond length for strongly localized HMAs or (2) weaken the localization of the mismatched atom from atom species. We found that incorporating larger atoms with the most thermodynamic favorable distribution invokes both approaches.

B. BAC and NN arrangement

The behavior of HMAs when adding a larger atom species with correspondingly weaker electronegativity (Sn or In) was also studied, particularly with attention to atom arrangements. Supercells of $B_{0.047}Ga_{0.812}In_{0.141}As$ with three B and nine In atoms, $Ge_{0.961}C_{0.008}Sn_{0.031}$ with one C and 4 Sn, and $Ga_{0.937}In_{0.063}N_{0.016}As_{0.984}$ with one N and four In were studied in various arrangements. For each arrangement, ion structures were re-relaxed, and the fully relaxed lattice constant was calculated as discussed in Sec. II. For the discussion below, $1NN_{max}$ refers to the arrangement in which the two species of atoms with the maximum difference in electronegativity are arranged in first-nearest neighboring sites. For example, in GeCSn and GaInNAs, $1NN_{max}$ arrangement means C–Sn and N–In (respectively) are directly bonded to each other. On the other hand, B and In are both group III atoms, so $1NN_{max}$ arrangement for BGaInAs means B and In on the nearest group III sites, still separated by an As atom.

We found that the most stable arrangements, with the lowest system energies, were those where the largest atoms were as close as possible to the smallest (most-mismatched) atoms, i.e., moving to the right in Fig. 4(a). Bandgaps consistently increased during the rearrangements as shown in Fig. 4(b). This agrees with the experimental blueshift observed upon annealing in both GaInNAs and BGaInAs, indicating atom rearrangements from random alloys in as-grown to In–N (In–B) nearest neighbors favored structures upon annealing.[41,42,60–62] The mechanisms that lead to the increase in the bandgap are slightly different. The lattice constants increased in both GeCSn and GaInNAs but decreased in BGaInAs as shown in Fig. 4(c). In GeCSn and GaInNAs, the local bonds transformed from Ge–C (Ga–N) dominated to Sn–C (In–N) dominated with longer bond length, increasing the overall lattice constant of the alloy. We noted that the lattice constant for four Sn in $1NN_{MAX}$ was much larger than other configurations, probably because Sn atoms were close enough to push against each other. As shorter bond lengths make it easier for the localized state to perturb the host conduction band, longer bond lengths raise the bar for charge to transfer from loosely bonded atoms to tightly bonded atoms. Subsequently, the bandgap reduction due to BAC decreased. However, the lattice constant in BGaInAs slightly decreased with decreased local bond length. Since strain has a larger effect and is decoupled from BAC in BGaInAs, the reduced lattice constant helped increase the bandgap in BGaInAs when rearranged to increase In in $1NN_{max}$ sites.

In addition, we found that the localization of small, mismatched atoms weakened during the rearrangement. As shown in Fig. 5, changing from no $1NN_{max}$ atoms to maximum $1NN_{max}$ decreases the charge density near the mismatched C, N, and B atoms, while the rest of the supercell showed an increase in the charge density. This represents the transformation of the charge from being localized on the mismatched atom to being more

25 March 2024 19:09:40

© Author(s) 2024

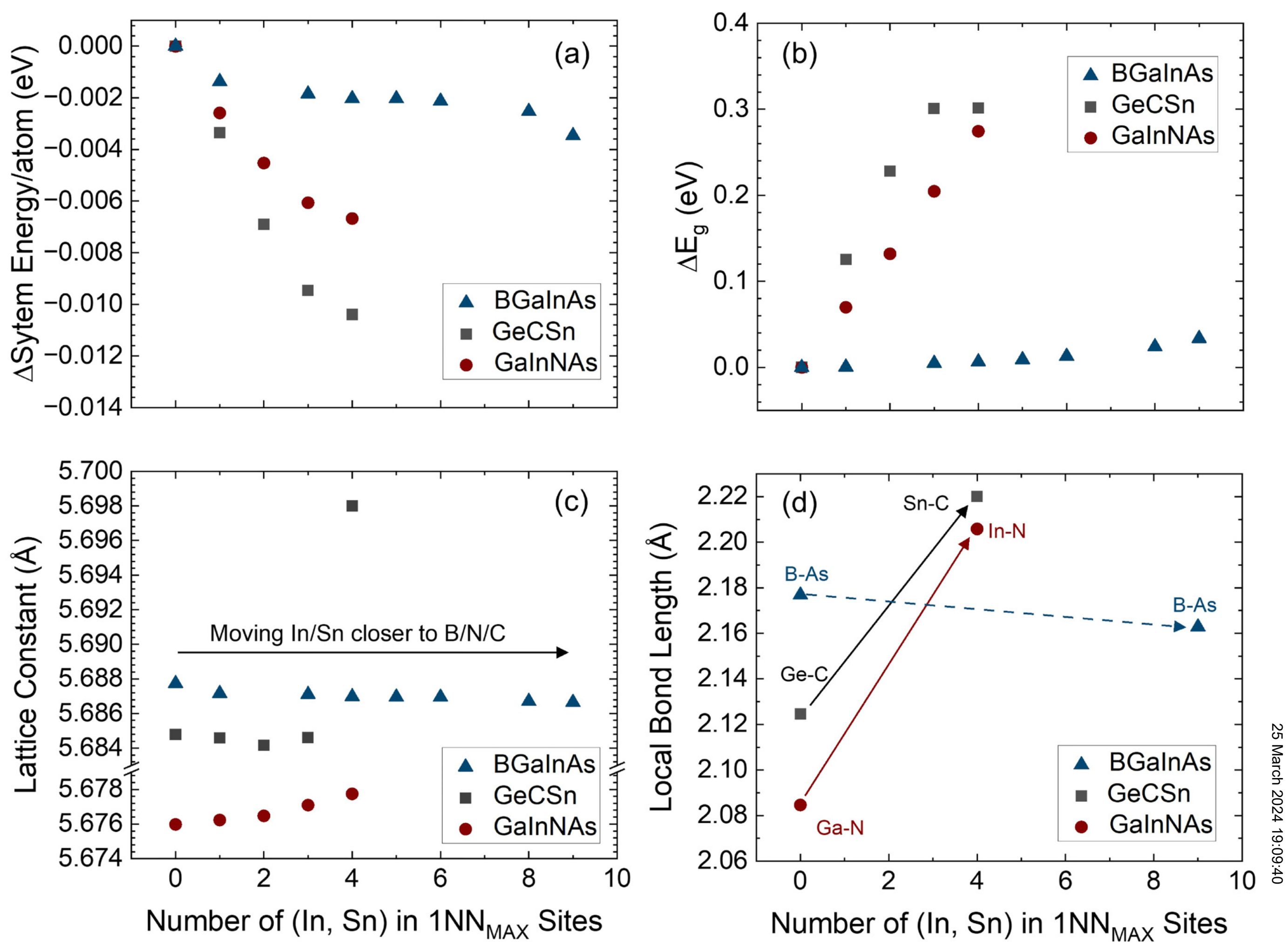

FIG. 4. Effects of rearrangement of largest atoms (In, Sn, and In) relative to the mismatched/smallest atom (B, C, N) in $B_3Ga_{52}In_9As_{64}$, $Ge_{123}C_1Sn_4$, and $Ga_{60}In_4N_1As_{63}$, respectively. Compositions are constant; only atom arrangements are changed. (a) Change in the total system energy, (b) change in the bandgap, (c) overall lattice constant, (d) local bond lengths, individually labeled.

delocalized over the entire supercell. We attribute this to the screening of the electrostatic potential on the highly mismatched atom by the larger, more loosely bound electron clouds from the less-electronegative atoms (Sn, In). The compensated electrons between species with the strongest electronegativity and weakest electronegativity balanced the wavefunction concentration. It is worth noting that the charge density of GeCSn and GaInNAs was concentrated along the lines of C/N atoms of neighboring supercells but was sparse in other regions. This phenomenon was not observed in BGaInAs. This might be because the C or N atom is partly localized, leading to perturbations extending across several bonds in the direction of the nearest mismatched atoms.

A longer local bond length in GeCSn and GaInNAs and the screening effect in all three mismatched alloys weakened the ability of C/B/N to cause BAC in GeSn/InGaAs. In the BAC model, the energy separation between E_- and E_+ indicates the strength of the interaction between the CB and mismatched atom state. As shown in Fig. 6(a), the energy differences between E_- and E_+ decreased moving from the fewest $1NN_{max}$ to most $1NN_{max}$, leading to a decrease in the bandgap. The maximum change in E_- and E_+ differences is only 0.13 eV, compared with 0.29 eV (0.33 eV) in GaInNAs (GeCSn), indicating that screening by the large atom (In) has a much smaller effect in BGaInAs than the other alloys. The delocalization of the wavefunction due to the screen effect also made the perturbed CBM in HMAs more resemble the unperturbed host CBM.

To further evaluate the similarity between perturbed CBs in HMAs and host CBM, the overlap integral of the wavefunction was

25 March 2024 19:09:40

© Author(s) 2024

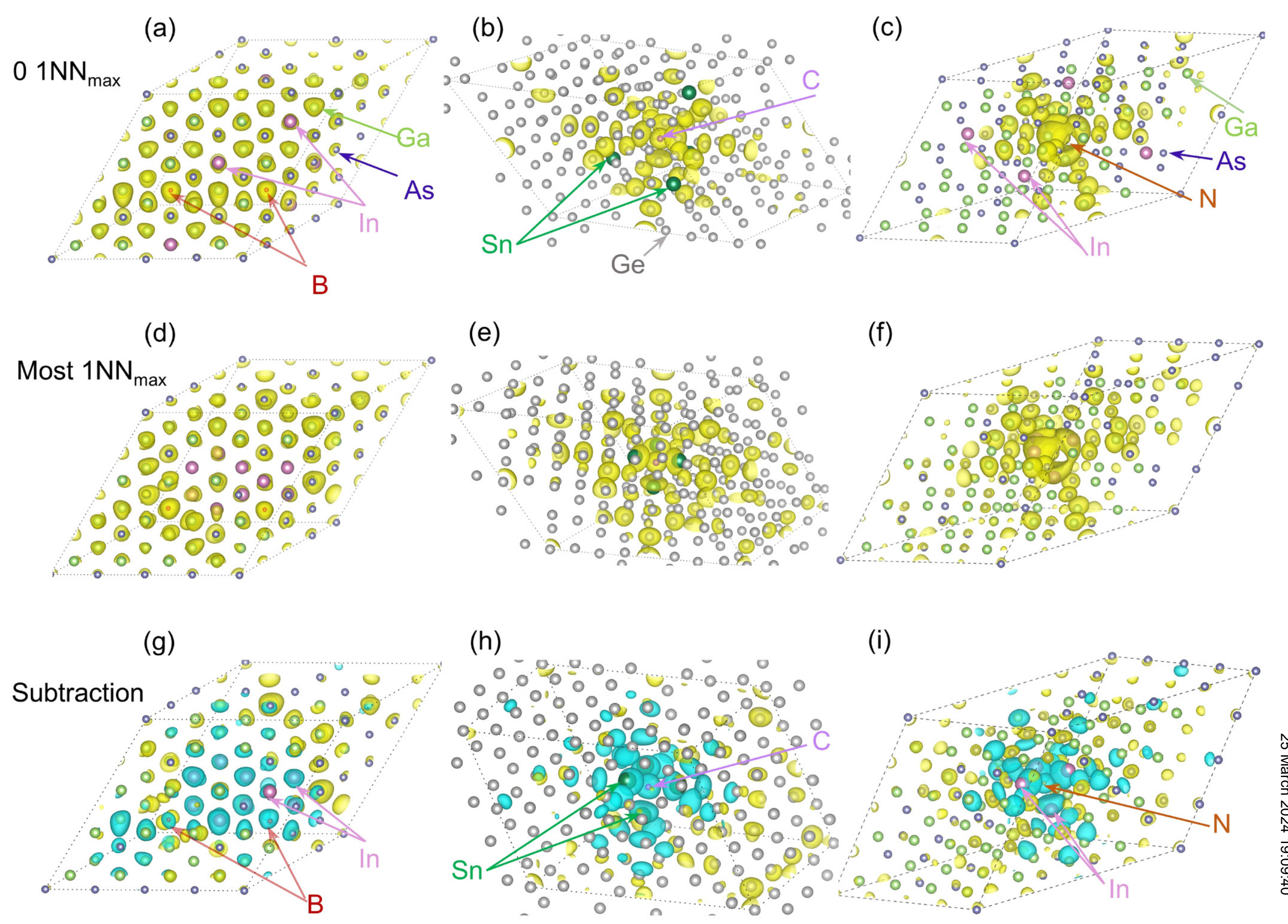

FIG. 5. (a)–(c) Charge density at the CBM with fewest $1NN_{max}$ for (a) BGaInAs, (b) GeCSn, (c) GaInNAs. (d)–(f) Charge density at the CBM with most $1NN_{max}$ for (d) BGaInAs, (e) GeCSn, (f) GaInNAs. (g)–(i) Change in the charge density at the CBM between states with most $1NN_{max}$ vs fewest 1NNmax for (g) BGaInAs, (h) GeCSn, (i) GaInNAs. Blue shows the regions where electron charge increases in arrangements with the fewest 1NNmax; yellow shows the increase in the charge in regions with the most 1NNmax.

25 March 2024 19:09:40

calculated. Although there were differences in the volumes of the host supercell and the HMAs supercell, it is important to note that the calculations considered a small fraction of alloying, leading to minimal volume disparities between the host supercell and HMAs, with a maximum difference of about 0.4%. These variations had a minimal influence on the results of the overlap integrals. The wavefunction overlap was calculated using similar methods as described in Ref. 28. The wavefunction $\psi_{n,k}(\vec{r})$ of a state in position r at wave vector k and band n can be expressed in the form of plane wave basis set as

$$\psi_{n,\,k}(\vec{r}) = \sum_{G} a_{n,G} e^{-i(\vec{G}+\vec{k})\bullet\vec{r}}, \tag{2}$$

where $a_{n,G}$ is the plane wave expansion coefficients at band n and wavevector k extracted from VASP's WAVECAR output file using WaveTrans or vaspwfc.[63] G is the set of lattice points in reciprocal space. All G values are examined in the range of

$$|G + \ k| \leq G_{cut} \equiv \sqrt{2mE_{max}}\,/\hbar, \tag{3}$$

where m is the mass of the particle, $E_{\max}$ is the plane wave cutoff energy, and $\hbar$ is the reduced Planck constant.

The overlap integral between states $\psi_{n,k}(\vec{r})$ and $\phi_{m,k}(\vec{r})$ at same k with the same basis set can then be expressed as

$$\langle \psi_{n,k} | \phi_{m,k} \rangle = \delta_{G_1 G_2} \sum_{G_1} \sum_{G_2} a^{*}_{n,G_1} b_{m,G_2}, \tag{4}$$

where a_{n,G_2} and b_{m,G_2} are the plane wave coefficients of $\psi_{n,k}(\vec{r})$ and

© Author(s) 2024

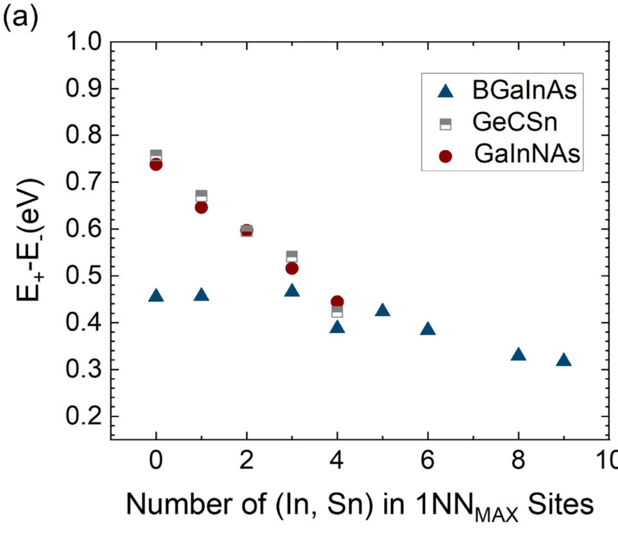

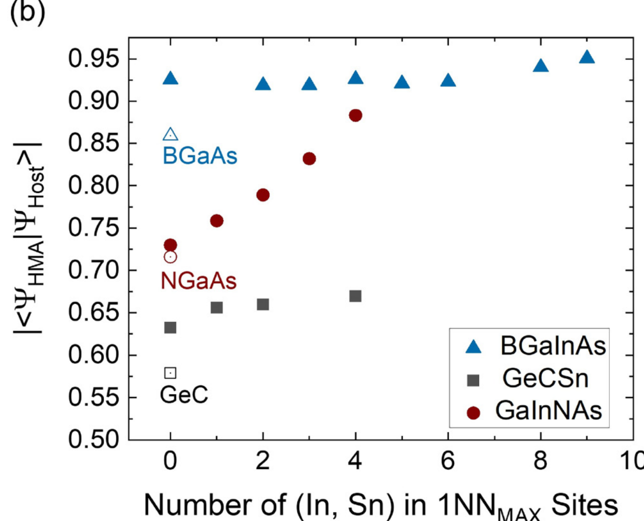

FIG. 6. (a) Energy differences between E_+ and E_- states in BGaInAs, GeCSn, and GaInNAs, (b) Wavefunction overlap of the CBM of Γ between BGa(In)As and fully relaxed GaAs, GeC(Sn) and Ge, Ga(In)NAs, and GaAs.

$\phi_{m,k}(\vec{r})$, respectively, and δ is the Kronecker delta function. Additionally, if the two states used different basis sets in k, the overlap integral was calculated in real space over the entire supercell as follows, with wavefunctions extracted by PyVaspwfc:[56]

$$\langle \psi_{n,k}|\phi_{m,k}\rangle = \iiint \psi^*_{n,k}(\vec{r})\phi_{m,k}(\vec{r})d^3r. \tag{5}$$

Since the wavefunction is not perfectly normalized from the VASP output,[64] the plane wave coefficients at each k were independently normalized as described in Ref. 28. We note here that the wavefunction extracted from VASP WAVECAR does not strictly represent the complete wavefunction due to the use of PAW approximation for handling core electrons with a pseudo-potential. However, given that the core electrons have relatively minimal influence on optoelectronic properties compared with valence electrons,[65] the extracted wavefunction remains a valuable approximation, particularly when comparing relative changes in the wavefunction across different configurations.

As shown in Fig. 6(b), with more $1NN_{max}$, the overlap of CBMs between HMAs and their host increased, especially for GeCSn and GaInNAs. It is worth noting that, even without NN rearrangement, the CBMs of BGaInAs, GeCSn, and GaInNAs were less perturbed than same concentration BGaAs, GeC, and GaNAs.

Finally, the energy, lattice, and bandgap change in BGaInAs during rearrangement were found to be much smaller than in GeCSn and GaInNAs. The distance of the shortest bonding length involved in rearrangement along with the electronegativity differences decided the upper limitation of bandgap change. In GeCSn and GaInNAs, the rearranged elements, C–Sn and N–In, were directly bonded to each other in the most stable structures with bonding lengths of 2.22 and 2.21 Å and a maximum of four Sn and In atoms. For BGaInAs, B and In atoms were bonded via As in a bond distance of 4.82 Å, although B can have a maximum number of surrounding In atoms of 12. In addition, the electronegativity difference is only 0.26 eV between B and In, compared with 0.41 eV between C and Sn, and 1.26 eV between N and In. The larger rearrangement distance plus the smaller electronegativity differences in BGaInAs limited the energy change in BGaInAs. Indeed, the experimental blueshift in BGaInAs quantum wells (QWs) with anneal is much smaller than in GaInNAs QWs with even larger In concentration.[61,62]

25 March 2024 19:09:40

IV. CONCLUSIONS

The band anticrossing (BAC) behavior of three different highly mismatched alloys (HMAs) has been studied to compare the effects of mismatch in anions (BGaAs), fully covalent atoms (GeC), and cations (GaAsN). We found that bandgap decreased with the addition of C and N but increased with B. This difference is because 1) C/N atoms more strongly localize the electron state and cause strong BAC, while B adds only weak localization; and 2) the BAC is coupled with local bond length change for strongly localized atoms, such as N and C, so a shorter bond length correlates with stronger coupling between the localized atom and the host band, further decreasing the bandgap. For BGaAs, BAC is almost decoupled from the bond length and shows weakly localized B states. For BGaAs, BAC was so weak that the bandgap increased slightly with B, as the slight decrease in the overall lattice constant had a stronger effect than the CB splitting effect from BAC.

Furthermore, BAC was inhibited in all HMAs by adding larger atoms with weaker electronegativity, such as In or Sn, particularly if the smallest and largest atoms are arranged as the first-nearest neighbors ($1NN_{max}$ positions). The $1NN_{max}$ arrangements

© Author(s) 2024

were energetically favorable and, thus, likely to occur with post-growth annealing. This weakening of BAC effects with $1NN_{max}$ rearrangement can be attributed to the changes in structural distortion and wavefunction delocalization due to the screening effects of the strongly electronegative, highly mismatched atom by the new weakly electronegative atoms. As a result, the bandgap consistently increased in BGaInAs, GeCSn, and GaInNAs with nearest-neighbor rearrangement toward $1NN_{max}$. Additionally, this rearrangement in BGaInAs tended to decrease the overall lattice constant, which also increased the bandgap. Therefore, the overall bandgap change in BGaInAs during rearrangement was much smaller than GeCSn or GaInNAs, which was likely due to the rearrangement in BGaInAs in the third shell of neighboring atoms and the weak localization of B in GaAs.

ACKNOWLEDGMENTS

This work was also supported by the National Science Foundation (NSF) (Award Nos. ECCS-1933836, DMR-1508646, and CBET-1438608). The authors also acknowledge the Learning, Exploration, Analysis, and Processing (LEAP) cluster at Texas State University for computing resources. This work was performed, in part, at the University of Texas Microelectronics Research Center, a member of the National Nanotechnology Coordinated Infrastructure (NNCI), which is supported by the NSF (No. ECCS-1542159). This work was also supported by NSF Partnership for Research and Education and Materials (PREM) Center at Texas State University under No. DMR-2122041.

AUTHOR DECLARATIONS

Conflict of Interest

The authors have no conflicts to disclose.

Author Contributions

Qian Meng: Conceptualization (equal); Data curation (equal); Formal analysis (equal); Investigation (equal); Methodology (equal); Resources (equal); Software (equal); Validation (equal); Visualization (equal); Writing – original draft (lead); Writing – review & editing (equal). **Seth R. Bank:** Conceptualization (equal); Data curation (equal); Formal analysis (equal); Funding acquisition (equal); Investigation (equal); Methodology (supporting); Resources (equal); Supervision (equal); Validation (equal); Visualization (equal); Writing – original draft (supporting); Writing – review & editing (supporting). **Mark A. Wistey:** Conceptualization (equal); Data curation (equal); Formal analysis (equal); Funding acquisition (equal); Investigation (equal); Methodology (equal); Resources (equal); Software (equal); Supervision (equal); Validation (equal); Visualization (equal); Writing – original draft (equal); Writing – review & editing (equal).

DATA AVAILABILITY

The data that support the findings of this study are available from the corresponding author upon reasonable request.

REFERENCES

[1] W. Shan, W. Walukiewicz, J. W. Ager, E. E. Haller, J. F. Geisz, D. J. Friedman, J. M. Olson, and S. R. Kurtz, "Band anticrossing in GaInNAs alloys," Phys. Rev. Lett. **82**(6), 1221–1224 (1999).

[2] J. Wu, W. Shan, and W. Walukiewicz, "Band anticrossing in highly mismatched III V semiconductor alloys," Semicond. Sci. Technol. **17**(8), 860–869 (2002).

[3] S. Francoeur, M.-J. Seong, A. Mascarenhas, S. Tixier, M. Adamcyk, and T. Tiedje, "Band gap of $GaAs_{1-x}Bi_x$, 0<x<3.6%," Appl. Phys. Lett. **82**(22), 3874–3876 (2003).

[4] K. M. Yu, W. Walukiewicz, J. Wu, W. Shan, J. W. Beeman, M. A. Scarpulla, O. D. Dubon, and P. Becla, "Diluted II-VI oxide semiconductors with multiple band gaps," Phys. Rev. Lett. **91**(24), 246403 (2003).

[5] K. M. Yu, W. Walukiewicz, J. W. Ager, D. Bour, R. Farshchi, O. D. Dubon, S. X. Li, I. D. Sharp, and E. E. Haller, "Multiband GaNAsP quaternary alloys," Appl. Phys. Lett. **88**(9), 092110 (2006).

[6] D. B. Jackrel, S. R. Bank, H. B. Yuen, M. A. Wistey, J. S. Harris, A. J. Ptak, S. W. Johnston, D. J. Friedman, and S. R. Kurtz, "Dilute nitride GaInNAs and GaInNAsSb solar cells by molecular beam epitaxy," J. Appl. Phys. **101**(11), 114916 (2007).

[7] N. López, L. A. Reichertz, K. M. Yu, K. Campman, and W. Walukiewicz, "Engineering the electronic band structure for multiband solar cells," Phys. Rev. Lett. **106**(2), 028701 (2011).

[8] C. A. Broderick, M. Usman, S. J. Sweeney, and E. P. O'Reilly, "Band engineering in dilute nitride and bismide semiconductor lasers," Semicond. Sci. Technol. **27**(9), 094011 (2012).

[9] T. Tanaka, S. Kusaba, T. Mochinaga, K. Saito, Q. Guo, M. Nishio, K. M. Yu, and W. Walukiewicz, "Molecular beam epitaxial growth and optical properties of highly mismatched $ZnTe_{1-x}O_x$ alloys," Appl. Phys. Lett. **100**(1), 011905 (2012).

[10] C. A. Stephenson, W. A. O'Brien, M. W. Penninger, W. F. Schneider, M. Gillett-Kunnath, J. Zajicek, K. M. Yu, R. Kudrawiec, R. A. Stillwell, and M. A. Wistey, "Band structure of germanium carbides for direct bandgap silicon photonics," J. Appl. Phys. **120**(5), 053102 (2016).

[11] K. M. McNicholas, R. H. El-Jaroudi, and S. R. Bank, "Kinetically limited molecular beam epitaxy of $B_xGa_{1-x}As$ alloys," Cryst. Growth Des. **21**(11), 6076–6082 (2021).

[12] R. H. El-Jaroudi, K. M. McNicholas, H. S. Mączko, R. Kudrawiec, and S. R. Bank, "Growth advancement of GaAs-based BGaInAs alloys emitting at 1.3 μm by molecular beam epitaxy," Cryst. Growth Des. **22**(6), 3753–3759 (2022).

[13] J. A. Van Vechten and T. K. Bergstresser, "Electronic structures of semiconductor alloys," Phys. Rev. B **1**(8), 3351–3358 (1970).

[14] M. Weyers, M. Sato, and H. Ando, "Red shift of photoluminescence and absorption in dilute GaAsN alloy layers," Jpn. J. Appl. Phys. **31**(7A), L853 (1992).

[15] W. G. Bi and C. W. Tu, "Bowing parameter of the band-gap energy of GaN_xAs_{1-x}," Appl. Phys. Lett. **70**(12), 1608–1610 (1997).

[16] N. G. Szwacki and P. Bogusławski, "GaAs:N vs GaAs:B alloys: Symmetry-induced effects," Phys. Rev. B **64**(16), 161201 (2001).

[17] S. Francoeur, M. J. Seong, M. C. Hanna, J. F. Geisz, A. Mascarenhas, H. P. Xin, and C. W. Tu, "Origin of the nitrogen-induced optical transitions in $GaAs_{1-x}N_x$," Phys. Rev. B **68**(7), 075207 (2003).

[18] P. R. C. Kent and A. Zunger, "Theory of electronic structure evolution in GaAsN and GaPN alloys," Phys. Rev. B **64**(11), 115208 (2001).

[19] T. Dannecker, Y. Jin, H. Cheng, C. F. Gorman, J. Buckeridge, C. Uher, S. Fahy, C. Kurdak, and R. S. Goldman, "Nitrogen composition dependence of electron effective mass in $GaAs_{1-x}N_x$," Phys. Rev. B **82**(12), 125203 (2010).

[20] A. Lindsay and E. P. O'Reilly, "Unification of the band anticrossing and cluster-state models of dilute nitride semiconductor alloys," Phys. Rev. Lett. **93**(19), 196402 (2004).

[21] E. P. O. Reilly, A. Lindsay, and S. Fahy, "Theory of the electronic structure of dilute nitride alloys: Beyond the band-anti-crossing model," J. Phys.: Condens. Matter **16**(31), S3257–S3276 (2004).

25 March 2024 19:09:40

© Author(s) 2024

[22]C. Skierbiszewski, P. Perlin, P. Wisniewski, W. Knap, T. Suski, W. Walukiewicz, W. Shan, K. M. Yu, J. W. Ager, E. E. Haller, J. F. Geisz, and J. M. Olson, "Large, nitrogen-induced increase of the electron effective mass in $InyGa_{1-y}NxAs_{1-x}$," Appl. Phys. Lett. **76**(17), 2409–2411 (2000).
[23]S. Fahy and E. P. O'Reilly, "Intrinsic limits on electron mobility in dilute nitride semiconductors," Appl. Phys. Lett. **83**(18), 3731–3733 (2003).
[24]W. Walukiewicz, W. Shan, K. M. Yu, J. W. Ager, E. E. Haller, I. Miotkowski, M. J. Seong, H. Alawadhi, and A. K. Ramdas, "Interaction of localized electronic states with the conduction band: Band anticrossing in II-VI semiconductor ternaries," Phys. Rev. Lett. **85**(7), 1552–1555 (2000).
[25]I. A. Buyanova, M. Izadifard, A. Kasic, H. Arwin, W. M. Chen, H. P. Xin, Y. G. Hong, and C. W. Tu, "Analysis of band anticrossing in Ga N_xP_{1-x} alloys," Phys. Rev. B **70**(8), 085209 (2004).
[26]K. Alberi, O. D. Dubon, W. Walukiewicz, K. M. Yu, K. Bertulis, and A. Krotkus, "Valence band anticrossing in $GaBixAs_{1-x}$," Appl. Phys. Lett. **91**(5), 051909 (2007).
[27]K. Alberi, J. Wu, W. Walukiewicz, K. M. Yu, O. D. Dubon, S. P. Watkins, C. X. Wang, X. Liu, Y.-J. Cho, and J. Furdyna, "Valence-band anticrossing in mismatched III-V semiconductor alloys," Phys. Rev. B **75**(4), 045203 (2007).
[28]I. A. Gulyas, C. A. Stephenson, Q. Meng, S. R. Bank, and M. A. Wistey, "The carbon state in dilute germanium carbides," J. Appl. Phys. **129**(5), 055701 (2021).
[29]A. C. Kirwan, S. Schulz, and E. P. O'Reilly, "Nature of the band gap of Ge:C alloys: Insights from hybrid functional density functional theory calculations," Semicond. Sci. Technol. **34**(7), 075007 (2019).
[30]C. A. Broderick, M. D. Dunne, D. S. P. Tanner, and E. P. O'Reilly, "Electronic structure evolution in dilute carbide Ge_{1-x} C_x alloys and implications for device applications," J. Appl. Phys. **126**(19), 195702 (2019).
[31]K. M. McNicholas, *Emerging Epitaxial Materials for Coherent III-V (Opto) Electronic Heterostructure Devices* (The University of Texas at Austin, 2019).
[32]Q. Meng, R. H. El-Jaroudi, R. C. White, T. Dey, M. S. Reza, S. R. Bank, and M. A. Wistey, "Effects of B and In on the band structure of BGa(In)As alloys," J. Appl. Phys. **132**(19), 193104 (2022).
[33]T. Hofmann, M. Schubert, G. Leibiger, and V. Gottschalch, "Electron effective mass and phonon modes in GaAs incorporating boron and indium," Appl. Phys. Lett. **90**(18), 182110 (2007).
[34]A. Lindsay and E. P. O'Reilly, "Theory of conduction band dispersion in dilute B_x $Ga_{1-x}As$ alloys," Phys. Rev. B **76**(7), 075210 (2007).
[35]G. L. W. Hart and A. Zunger, "Electronic structure of BAs and boride III-V alloys," Phys. Rev. B **62**(20), 13522–13537 (2000).
[36]W. Shan, W. Walukiewicz, J. Wu, K. M. Yu, J. W. Ager, S. X. Li, E. E. Haller, J. F. Geisz, D. J. Friedman, and S. R. Kurtz, "Band-gap bowing effects in $B_xGa_{1-x}As$ alloys," J. Appl. Phys. **93**(5), 2696–2699 (2003).
[37]G. Leibiger, V. Gottschalch, V. Riede, M. Schubert, J. N. Hilfiker, and T. E. Tiwald, "Interband transitions and phonon modes in $B_xGa_{1-x}As$ (0<~x<~0.03) and GaN_yAs_{1-y} (0<~y<~0.037): A comparison," Phys. Rev. B **67**(19), 195205 (2003).
[38]S. Ilahi, F. Saidi, R. Hamila, N. Yacoubi, H. Maaref, and L. Auvray, "Shift of the gap energy and thermal conductivity in BGaAs/GaAs alloys," Phys. B **421**, 105–109 (2013).
[39]T. Hidouri, S. Nasr, and F. Saidi, "Experimental and theoretical study of novel BGaAs/GaAs single quantum well for photonic applications," Vacuum **173**, 109182 (2020).
[40]R. Kudrawiec, M. P. Polak, K. M. McNicholas, J. Kopaczek, M. A. Wistey, and S. R. Bank, "Bowing of the band gap and spin-orbit splitting energy in BGaAs," Mater. Res. Express **6**(12), 125913 (2020).
[41]V. Lordi, V. Gambin, S. Friedrich, T. Funk, T. Takizawa, K. Uno, and J. S. Harris, "Nearest-neighbor configuration in (GaIn)(NAs) probed by x-ray absorption spectroscopy," Phys. Rev. Lett. **90**(14), 145505 (2003).
[42]P. J. Klar, H. Grüning, J. Koch, S. Schäfer, K. Volz, W. Stolz, W. Heimbrodt, A. M. K. Saadi, A. Lindsay, and E. P. O'Reilly, "(Ga, In)(N, As)-fine structure of the band gap due to nearest-neighbor configurations of the isovalent nitrogen," Phys. Rev. B **64**(12), 121203 (2001).
[43]A. Lindsay and E. P. O'Reilly, "Theory of electronic structure of BGaAs and related alloys," Phys. Status Solidi (C) **5**(2), 454–459 (2008).
[44]G. Kresse and J. Furthmüller, "Efficient iterative schemes for *ab initio* total-energy calculations using a plane-wave basis set," Phys. Rev. B **54**(16), 11169–11186 (1996).
[45]P. E. Blöchl, "Projector augmented-wave method," Phys. Rev. B **50**(24), 17953–17979 (1994).
[46]J. Heyd, G. E. Scuseria, and M. Ernzerhof, "Hybrid functionals based on a screened Coulomb potential," J. Chem. Phys. **118**(18), 8207–8215 (2003).
[47]J. Heyd, J. E. Peralta, G. E. Scuseria, and R. L. Martin, "Energy band gaps and lattice parameters evaluated with the Heyd-Scuseria-Ernzerhof screened hybrid functional," J. Chem. Phys. **123**(17), 174101 (2005).
[48]C. Freysoldt, B. Grabowski, T. Hickel, J. Neugebauer, G. Kresse, A. Janotti, and C.G. Van de Walle, "First-principles calculations for point defects in solids," Rev. Mod. Phys. **86**(1), 253–305 (2014).
[49]I. Gulyas, R. Kudrawiec, and M. A. Wistey, "Electronic structure of $BxGa_{1-x}As$ alloys using hybrid functionals," J. Appl. Phys. **126**(9), 095703 (2019).
[50]F. D. Murnaghan, "Finite deformations of an elastic solid," Am. J. Math. **59**(2), 235–260 (1937).
[51]F. Birch, "Finite elastic strain of cubic crystals," Phys. Rev. **71**(11), 809–824 (1947).
[52]T. B. Boykin, N. Kharche, G. Klimeck, and M. Korkusinski, "Approximate bandstructures of semiconductor alloys from tight-binding supercell calculations," J. Phys.: Condens. Matter **19**(3), 036203 (2007).
[53]V. Popescu and A. Zunger, "Extracting E versus k → effective band structure from supercell calculations on alloys and impurities," Phys. Rev. B **85**(8), 085201 (2012).
[54]P. V. C. Medeiros, S. Stafström, and J. Björk, "Effects of extrinsic and intrinsic perturbations on the electronic structure of graphene: Retaining an effective primitive cell band structure by band unfolding," Phys. Rev. B **89**(4), 041407 (2014).
[55]P. V. C. Medeiros, S. S. Tsirkin, S. Stafström, and J. Björk, "Unfolding spinor wave functions and expectation values of general operators: Introducing the unfolding-density operator," Phys. Rev. B **91**(4), 041116 (2015).
[56]Q. Zheng, see https://github.com/QijingZheng/VaspBandUnfolding for VaspBandUnfolding.
[57]H. P. Hjalmarson, P. Vogl, D. J. Wolford, and J. D. Dow, "Theory of substitutional deep traps in covalent semiconductors," Phys. Rev. Lett. **44**(12), 810–813 (1980).
[58]Q. Meng *et al.*, "Electronic structure evolution in BGaAs alloys" (unpublished).
[59]S.-H. Wei and A. Zunger, "Giant and composition-dependent optical bowing coefficient in GaAsN alloys," Phys. Rev. Lett. **76**(4), 664–667 (1996).
[60]H. P. Xin, K. L. Kavanagh, Z. Q. Zhu, and C. W. Tu, "Observation of quantum dot-like behavior of GaInNAs in GaInNAs/GaAs quantum wells," Appl. Phys. Lett. **74**(16), 2337–2339 (1999).
[61]V. Lordi, H. B. Yuen, S. R. Bank, M. A. Wistey, J. S. Harris, and S. Friedrich, "Nearest-neighbor distributions in $Ga_{1-x}In_xNyAs_{1-y}$ and $Ga_{1-x}In_xN_yAs_{1-y-z}Sb_z$ thin films upon annealing," Phys. Rev. B **71**(12), 125309 (2005).
[62]R. H. El-Jaroudi, K. M. McNicholas, A. F. Briggs, S. D. Sifferman, L. Nordin, and S. R. Bank, "Room-temperature photoluminescence and electroluminescence of 1.3-μm-range BGaInAs quantum wells on GaAs substrates," Appl. Phys. Lett. **117**(2), 021102 (2020).
[63]R. M. Feenstra, N. Srivastava, Q. Gao, M. Widom, B. Diaconescu, T. Ohta, G. L. Kellogg, J. T. Robinson, and I. V. Vlassiouk, "Low-energy electron reflectivity from graphene," Phys. Rev. B **87**(4), 041406 (2013).
[64]G. Kresse and D. Joubert, "From ultrasoft pseudopotentials to the projector augmented-wave method," Phys. Rev. B **59**(3), 1758–1775 (1999).
[65]R. M. Martin, *Electronic Structure: Basic Theory and Practical Methods* (Cambridge University Press, 2020).

25 March 2024 19:09:40

© Author(s) 2024